EUROPEAN FUSION DEVELOPMENT AGREEMENT

EFDA–JET–PR(04)45

T. Hellsten, M. Laxåback, T. Bergkvist, T. Johnson, F. Meo, F. Nguyen, C.C. Petty, M. Mantsinen, G. Matthews, J.-M. Noterdaeme, T. Tala, D. Van Eester, P. Andrew, P. Beaumont, M. Brix, J. Brzozowski, L.-G. Eriksson, C. Giroud, E. Joffrin, V. Kiptily, J. Mailloux, M.-L. Mayoral, I. Monakhov, R. Sartori, A. Staebler, E. Rachlew, E. Tennfors, A. Tuccillo, A. Walden, V. Bobkov, K.-D. Zastrow and JET EFDA contributors

On the Parasitic Absorption in FWCD Experiments in JET ITB Plasmas

On the Parasitic Absorption in FWCD Experiments in JET ITB Plasmas

T. Hellsten[1], M. Laxåback[1], T. Bergkvist[1], T. Johnson[1], F. Meo[2], F. Nguyen[3], C.C. Petty[4], M. Mantsinen[5], G. Matthews[6], J.-M. Noterdaeme[7], T. Tala[6], D. Van Eester[9], P. Andrew[7], P. Beaumont[7], M. Brix[8], J. Brzozowski[1], L.-G. Eriksson[3], C. Giroud[7], E. Joffrin[3], V. Kiptily[7], J. Mailloux[7], M.-L. Mayoral[7], I. Monakhov[7], R. Sartori[10], A. Staebler[8], E. Rachlew[1], E. Tennfors[1], A. Tuccillo[11], A. Walden[7], V. Bobkov[8], K.-D. Zastrow[7] and JET EFDA contributors*

[1]Association VR-Euratom, Sweden,
[2]Association Euratom-Risø, National Laboratory, Denmark,
[3]Association Euratom-CEA, CEA-Cadarache, France,
[4]General Atomics, San Diego,USA.
[5]HUT, Association Euratom-Tekes, Finland,
[6]VTT Processes, Association Euratom-Tekes, Finland,
[7]UKAEA Fusion Association, Culham Science Centre, U.K.,
[8]Max-Planck-Institut für Plasmaphysik, EURATOM Association, Garching, Germany,
[9]LPP-ERM/KMS, Association Euratom-Belgian State, Belgium,
[10]EFDA CSU-Garching, Germany,
[11]Association Euratom-ENEA, Italy,

Preprint of Paper to be submitted for publication in
Nuclear Fusion

ABSTRACT

Fast wave current drive experiments have been performed in JET plasmas with electron internal transport barriers, eITB, produced with LHCD. Because of the large fraction of parasitic absorption, due to weak single pass damping, the inductive nature of the plasma current and the interplay between the RF-driven current and the bootstrap current only small changes are seen in the central current profiles. The measured difference in the central current density for co and counter current drive is larger than the response expected from current diffusion calculations, but smaller than the driven currents, suggesting a faster current diffusion than that given by neo-classical resistivity. A large fraction of the power is absorbed by cyclotron damping on residual ^{3}He ions and a significant fraction appears not to have been deposited in the plasma. The strong degradation of heating and current drive occurs simultaneously with strong increases in the BeII and CIV line intensities in the divertor. The degradation depends on the phasing of the antennas and increases with reduced single pass damping, consistent with RF-power being lost by dissipation of rectified RF-sheath potentials at the antennas and walls. Asymmetries in direct electron heating, lost power and production of impurities, fast ions and gamma-rays are seen for co and counter current drive. These differences are consistent with differences in the absorption on residual ^{3}He ions due to the RF-induced pinch. Effective direct electron heating, comparable to the indirect electron heating with H minority heating, is found for dipole phasing of the antennas without producing a significant fast ion pressure and with low impurity content in the divertor plasma.

1. INTRODUCTION

The use of non-inductive current drive with low frequency RF-waves to sustain and control the current in toroidal plasmas has the advantages of easy access of the waves to the high density plasma centre [1]. Fast Wave Current Drive, FWCD, is based on the acceleration of the guiding centres of electrons along the magnetic field lines by the mirror force, arising via the interaction of the magnetic moments with the parallel gradients in the magnetic field formed through compression of the field by the fast magnetosonic wave [2]; so called Transit Time Magnetic Pumping, TTMP. The acceleration by the mirror force gives rise to a parallel electric field counteracting the mirror force. The parallel electric field in turn gives rise to electron Landau damping, ELD. Since the mirror force and the parallel electric field are ant-parallel the cross terms in the dielectric tensor reduce the total damping to half of the original TTMP. The total damping, which increases with the electron gyro radius and density, is in general weak for present day tokamaks except at high beta. Efficient current drive requires high electron temperature and low density since the efficiency increases with decreasing collisionality. The presence of trapped electrons can strongly reduce the efficiency [3, 4]. Increasing the frequency or decreasing the parallel wave number, such that the phase velocity of the waves becomes much higher than the electron thermal velocity, reduces the interactions with trapped electrons. However, this also reduces the resonant fraction of the electrons

and hence the single pass damping, making the current drive sensitive to parasitic absorption by other damping mechanisms.

Plasmas with peaked electron temperature profiles give rise to peaked power deposition and, because of trapped particle effects, even further peaked driven current profiles. The strong localisation of the driven current near the magnetic axis makes fast wave current drive a potential tool for controlling the central current in tokamak plasmas. This is particularly important for plasmas with internal transport barriers with strongly reversed magnetic shear, in which current holes tend to form [5]. Fast wave electron heating also has the advantage over indirect electron heating via cyclotron heated high-energy ions of a prompt heating without increasing the fast ion pressure. Furthermore it has a peaked heating profile, something which is difficult to achieve with high-energy cyclotron heated ions with wide orbits.

Evidence of fast wave heating by TTMP/ELD was first seen at high ^{3}He concentrations with the A1 antennas at JET [6]. FWCD in the higher harmonic ion cyclotron frequency range has been carried out in DIII-D [7, 8] and in Tore Supra [9]. FWCD in plasmas with negative magnetic shear have been carried out in DIII-D [10]. In JET, heating at the frequency of the third harmonic D and ^{4}He resonances resulted in dominating cyclotron heating of the majority D ions [11] and of ^{4}He ions in a ^{4}He plasma with ^{4}He beams [12].

Because of the weak single pass damping by TTMP/ELD in present day experiments it is important to avoid parasitic absorption, in particular ion cyclotron absorption, which can damp a large fraction of the power and thereby substantially degrade the current drive efficiency. This restricts the suitable frequency ranges for FWCD to scenarios with either weak cyclotron damping or with strong TTMP/ELD [4]. However, parasitic power losses are often seen in connection with FWCD experiments even when the cyclotron absorption is weak, such as for frequencies below the cyclotron frequency of hydrogen. FWCD experiments in L-mode in DIII-D showed that the single pass damping had to exceed a value of the order of 8% for efficient current drive. Modelling of the current drive could be brought into agreement with experimental results in DIII-D [7] and in JET for third harmonic deuterium damping [11] by assuming an ad hoc parasitic loss term corresponding to 4% single pass damping. In DIII-D H-mode plasmas, the current drive efficiency was found to correlate strongly with the ELM frequency and less with the single pass damping [8].

The degradation of heating by parasitic power losses does not only depend on the scenario, but also on the antenna. A strong degradation was clearly seen with the JET A2 antennas for phasings coupling to modes with low toroidal mode numbers [13, 14]. Such strong degradation had not been seen for the A1 antennas under normal operating conditions [15]. However, strong reduction in the heating was seen with the A1 antennas for monopole phasing with large misalignment angles between the magnetic field lines and the Faraday screens in front of the antenna straps [16], giving rise to large impurity radiation by nickel [16] and beryllium [17]. The increased impurity accumulation was explained by sputtering caused by the presence of rectified RF-sheath potentials at the Faraday screens in front of the antennas [17, 18]. The increased radiation from nickel was seen to correlate

with the antenna voltage [18] and the parasitic losses could be explained by the presence of rectified RF-sheath potentials for field lines connecting with the screen and limiters of the antenna [17]. Sputtering caused by rectified RF-sheaths has also been proposed as an explanation for increases in metallic impurity during normal RF operation with small misalignment angles [19]. Impurity generation by far field effects has been observed in ASDEX Upgrade [20]. RF-sheath rectification is one of several mechanisms that have been proposed to explain the parasitic absorption under various conditions [19, 17]. In the limit of weak single pass damping the losses due to sheath rectification increases dramatically because of the inefficient coupling to non-resonant magnetosonic eigenmodes [21, 22]. This is a more severe problem for antenna phasings with narrow mode spectra. As a result a large fraction of the power can be lost at the RF-sheaths even for small misalignment angles.

FWCD experiments in plasmas with internal transport barriers carried out in JET are analysed in this paper. Because of the restricted power available for the JET ICRH system at lower frequencies, a frequency of 37MHz and a magnetic field of 3.45T at the magnetic axis was chosen for the study of fast wave heating and current drive in plasmas with electron internal transport barriers, eITB. For this choice of frequency and magnetic field the hydrogen cyclotron resonance passes outside the plasma on the low field side, the majority D-resonance is located at the far high field side and the ^{3}He resonance is close to the centre. Cyclotron absorption by ^{3}He can be reduced by either operating without ^{3}He or at a high concentration. Low minority concentrations result in cyclotron heating and intermediate concentrations in mode conversion located between the ^{3}He and D resonances. Mode conversion at the edge on the high field side of the D-resonance can cause parasitic absorption at low ^{3}He concentrations [4, 23]. For high ^{3}He concentrations the presence of a cut-off for the fast wave at the high field side of the ^{3}He resonance prevents the wave from reaching the cyclotron resonance of deuterium and the mode conversion region at the high field side. The parasitic absorption by a low minority concentration of ^{3}He has similarities with that of second harmonic tritium foreseen for FWCD in ITER [24] in that the resonance occurs at the same frequency and that the absorption is weak for thermal ions and increases with power. Unfortunately the TTMP/ELD damping is weak due to the low β-values in these experiments. Efficient fast wave heating is nevertheless obtained with dipole phasing in spite of the rather low single pass damping of the order of 3%. The heating efficiency is found to be similar for these plasmas as for hydrogen minority cyclotron heating, but with smaller sawtooth-like modes in the reversed shear region [25] and with a higher impurity content. Although the current drive efficiency in terms of ampere per watt absorbed on the electrons is fairly high, 0.07A/W for FWCD with +/–90° phasings, it is difficult to affect the plasma current. The main reasons are: the parasitic absorption, the strongly inductive nature of the plasma current due to the high electric conductivity at the high electron temperatures and the interplay between the fast wave driven current and the bootstrap current, which, due to the dependence of the bootstrap current on the poloidal magnetic field, decreases the bootstrap current as the driven current increases. The measured changes in central current density with the +90° and –90° phasings are

larger than those expected from the time dependent response when assuming neo-classical resistivity, but smaller than the calculated steady state current drive. Current diffusion faster than that given by neo-classical resistivity has in the past been seen on DIII-D [7]. A significant amount of the heating power is found to be lost as it is neither delivered to the divertor nor radiated into the main chamber. Such losses are consistent with losses caused by fast ions intercepted by the wall or by rectified RF-sheath potentials at the antennas and/or the wall. Absorption via mode conversion near the high field side edge and by beam ions are possible mechanisms for degrading the power depositions, but they seem to be small and would ultimately result in that the absorbed energy is either radiated away or transported to the divertor. Parasitic absorption by cyclotron damping on residual ^{3}He is observed and found to depend on the direction of propagation of the launched waves, consistent with the RF-induced spatial transport of resonant ions [26-28]. However, the estimated maximum amount of ^{3}He in the machine is not enough to explain the low direct electron damping. The parasitic power losses can neither be explained by any amount of ^{3}He, which indicates that losses due to RF sheath effects indeed play an important role. This conjecture is supported by BeII line radiation. Under conditions with weak single pass absorption with +90° and –90° phasings, the BeII line radiation in the divertor increases with an order of magnitude compared to the levels during dipole phasing or hydrogen minority heating.

The paper is organised as follows: In section 2 an overview of the experiments is given and experimental results are presented in section 3. Simulations of the experiments are presented in section 4. In section 5 the results are discussed and analysed and a summary is given in section 6.

2. OVERVIEW OF THE EXPERIMENTS

Most of the fast wave current drive and heating experiments presented here were carried out in deuterium ITB plasmas with strongly reversed central magnetic shear in a single-null divertor configuration with the following parameters: On axis magnetic field 3.45T, plasma current 2MA, elongation 1.65, minor radius a ≈ 0.9m and magnetic axis R_0 ≈ 3m. Hot low density plasmas, $n_e \approx 1.2\text{x}10^{19}\text{m}^{-3}$, with strongly reversed magnetic shear were created using nearly 3s of 2–2.5MW LHCD preheating at 3.7GHz. The LHCD preheat was switched off when around 13MW of NBI and up to 6MW of ICRF power was applied at t = 44s. During the application of NBI and RF-heating, the plasma current and toroidal field were kept constant. The time sequence of the coupled power and plasma parameters for a typical discharge can be seen in Fig. 1, note that the discharge starts at t = 40s. The RF power was applied at a frequency of 37MHz, placing the hydrogen resonance outside the plasma on the low field side and the deuterium resonance, $\omega = \omega_{CD}$, at $R \approx 2.10$m on the far high field side. The cyclotron resonance of ^{3}He, $\omega = \omega_{C3He}$, is located at about R = 2.8m and intersects the plasma near the magnetic axis. Cyclotron absorption on residual ^{3}He ions was detected in spite of the precautions taken to avoid ^{3}He in the plasma. The four strap A2 antennas were used with a phasing of +90° and –90° between adjacent current straps for driving currents respectively anti-parallel and parallel to the ohmic current. The asymmetric toroidal mode spectra peaked at

$n_\phi \approx +15$ for +90° and $n_\phi \approx -15$ for −90° phasing [29], where the toroidal direction is parallel to the ohmic current. Reference discharges were carried out at 37MHz with 180° phasing, so called dipole phasing, which produces a symmetric spectrum peaked at $n_\phi \approx \pm 25$, and at 51MHz for H-minority heating with a hydrogen to deuterium density ratio of 0.06 and a phasing of +90°. At 51MHz the hydrogen resonance, $\omega = \omega_{CH}$, passes through the midplane at about 3.1m. One reference shot without NBI was also made at 37MHz with +90° phasing.

The distance between antennas and the plasma boundary, the radial outer gap or ROG, was about 5cm. The angle between the Faraday screens and the magnetic field lines was about 7°. Square-wave modulations of the RF-power at a frequency of 20Hz and an amplitude variation of 50% were performed in order to measure the direct electron heating [30]. One power modulation period was applied in the early phase of the discharge and one in the later. The power deposition on electrons was obtained from Fourier analysis and break-in-slope analysis of the time resolved radial electron temperature profiles. These were measured from electron cyclotron emission, ECE, using a heterodyne radiometer with a time resolution of 0.5ms and a spatial uncertainty of ±5cm along the line-of-sight, which passes about 15cm below the midplane. Up to 70% of the power has in the past been accounted for using the same technique for discharges with similar RF-frequencies and high ^{3}He concentrations, dominated by mode conversion [31]. The power deposition measurements work best in the central parts of the plasma since the characteristic time scale for energy transport should be long compared to the period of the modulations for accurate results.

The ion temperature and toroidal rotation profiles of carbon were measured using active Charge eXchange Spectroscopy (CXS), with a radial resolution of 10cm [32]. The current profiles were obtained using the Motional Stark Effect (MSE), diagnostic, measuring the magnetic field pitch angle $\gamma = \tan^{-1}(B_Z/B_\phi)$ from the polarized, Doppler shifted, D_α emission from one of the heating beams [33]. Complementary information on the evolution of the current profile was obtained from EFIT equilibrium reconstructions constrained by data from the Faraday rotation obtained from eight lines-of-sight of the far-infrared polarimeter [34, 35].

The effect of reducing the misalignment angle was studied by changing the plasma current from 2MA to 2.8MA in one of the discharges in a series of ^{4}He-plasmas with 7.5MW of beam power. Because of the low beam power and low electron temperature the shear reversed phase was rapidly lost and large losses of power were seen for these discharges. In order to increase the electron temperature in these discharges one antenna was used for minority H-heating at 51MHz in dipole phasing with a power of about 1.5MW and the LHCD was maintained for a short period into the main heating phase. Due to the low hydrogen concentration in these ^{4}He plasmas, significant losses of fast hydrogen ions were detected with a probe located outside the plasma, measuring escaping MeV ions using activation technique [36].

3. EXPERIMENTAL RESULTS

Initially a plasma with high electron temperature, low density and strongly reversed magnetic shear

was created using LHCD preheat. When the NBI was applied the central density increased due to beam fuelling, resulting in a decrease in the electron temperature from about 8keV to 4.5keV, Fig.1. As the NBI and ICRH heating continued the electron temperature started to increase again and saturated around 8keV at $t \approx 45.5$s. Minor variations in the central electron temperature occurred because of sawtooth-like events produced by tearing modes appearing in the reversed magnetic shear region close to the $q = 3$ surface [25]. Direct electron heating produced small sawtooth-like modes. Larger, "mini-monster-like", sawteeth were produced in Pulse No: 58682 with hydrogen minority heating, Fig.2, indicating stabilisation by fast ions similar to the stabilisation of conventional sawteeth in the presence of a $q = 1$ surface [37]. Because of the presence of high-energy ^{3}He ions some stabilisation also occurred for heating at 37MHz, stronger for +90° phasing than for –90°. During the initial main heating phase the ion temperature increased from about 6keV to12keV at $t \approx 45.5$s. The evolution of the electron and ion temperature profiles are shown in Figs.3 and 4 for a typical Pulse No: 60664 with in average 5.3MW of RF heating at –90° phasing. Before $t = 47.4$s the foot of the internal transport barrier was located at about $R = 3.25$m, corresponding to $r/a = 0.28$. At $t \approx 47.4$s q_{min} reached 2 and the barrier expanded, following the outer $q = 2$ surface [38] to 3.45m, corresponding to $r/a = 0.5$, Fig.5. In this improved confinement regime the central ion temperature increased to over 20keV and the neutron yield triggered a step down of the NBI power, programmed in order to avoid a disruption in connection with the barrier expansion. After the step down the electron temperature continued to increase for a while, as can be seen in Fig.1, followed by a rapid decay at $t = 47.61$s caused by an MHD mode at the foot of the barrier. In this case the mode had an inversion radius $R = 3.43$m and was located near the $q = 2$ surface. The dynamics of the discharges was sensitive to small differences in the pre-heat, and also to the heating and possible current drive in the main phase, through changes in current diffusion rate, strength of the sawtooth like modes, bootstrap currents and transport in the barrier. For some discharges with good heating, such as Pulse No: 58682 and Pulse No: 60663, the improved heating increased the neutron yield above the preset limit, causing a step down in the NBI before q_{min} reached 2.

The evolutions of the electron temperature and density profiles were important for the direct electron absorption by TTMP/ELD and for the current drive efficiency. The stepping down of the NBI resulted in lower ion and electron temperatures and lower density in the core. This reduced the single pass damping and was expected to affect the heating efficiency. The heating performance of the reference discharges at 37MHz with dipole phasing and H minority heating at 51MHz with +90° phasing was clearly better than the FWCD at 37MHz with +90° and –90° phasing. Both reference scenarios produced similar plasmas for the same RF-power.

Data for relevant discharges is given in Table 1.

3.1 POWER ABSORBED BY DIRECT ELECTRON HEATING

The fraction of RF power that was directly absorbed on electrons, as deduced from the electron temperature response to the power modulation, varied strongly with plasma conditions and antenna

phasing. With dipole phasing over 20% of the total RF-power could be accounted for in the central part of the plasma, whereas for the +90° and the –90° phasings the fraction varied from a few percent up to 28%. The higher values were obtained at higher electron temperatures. The fractions absorbed on electrons are given in Table 1 for the first and second modulation phase. Measured direct electron heating power deposition profiles are shown in Fig.6. Note that although the coupled power for the dipole was about half of that for +/-90° the maximum absorption in the centre was comparable. The depositions are typically characterised by peaked profiles extending out to $r/a \approx 0.5$, and flatter profiles outside of that. While the power densities in the outer parts of the plasma were in general below the noise level, the power absorbed there can still be significant due to the large volume and it is possible that a part of the power was absorbed in connection with mode conversion near the high field side edge. The current driven outside the barrier will however be insignificant due to the low temperature and large fraction of trapped electrons there.

The sharply peaked deposition profiles in the centre lie mostly inside the transport barrier, where the transport broadening of the temperature response to the modulation should be small. Because of the more peaked pressure profiles these power depositions are more peaked than the rather flat profiles measured in sawtoothing discharges with positive magnetic shear just after a sawtooth crash [6].

The low fraction of power obtained from modulations suggests that a large fraction of the power was not absorbed by TTMP/ELD.

3.2 PRESENCE OF FAST ^{3}HE IONS

The presence of high-energy ^{3}He ions was confirmed by several methods: by a gamma-ray camera detecting collisions with C and Be impurities, by an RF-probe measuring cyclotron emission, by TAE mode excitation and by measuring the anisotropic energy content in the plasma.

High-energy ^{3}He ions were detected with gamma-ray emission spectroscopy [39] from peaks at 2.31MeV and at 4.4MeV, coming from $^{12}C(^3He, p+\gamma)^{14}N$ and $^9Be(^3He, p+\gamma)^{11}B$ reactions respectively. These peaks were clearer for the discharge without NBI, when the background of gamma-radiation was lower. The peak from the dominant $^{12}C(^3He, p+\gamma)^{14}N$ reaction could just be detected for the discharges with +90°–phasing and NBI, whereas it could not for the –90° discharges with NBI. The difference in peak gamma emission magnitude for the two phasings is consistent with the RF-induced pinch of resonant ions [26- 28]. Gamma-rays from the inelastic scattering of high-energy D ions against ^{12}C nuclei could not be detected, indicating that the power damped on deuterium was small. Such gamma-rays have previously been seen in mode conversion experiments with high ^{3}He-concentrations [31]. To determine the absolute density of ^{3}He from the gamma emission would require the knowledge of the carbon concentration and the fraction of ^{3}He ions with sufficiently high energy for the reactions.

An ion cyclotron emission peak at 26.5MHz, corresponding to the unshifted cyclotron resonance of ^{3}He at R = 4.0m, for B_0 = 3.45T, and consistent with the presence of high-energy ^{3}He ions at the

edge of the plasma, was detected in Pulse No: 58684 with a RF-heating power of 5.3MW. The peak was not detected in similar discharges at power levels around 4MW. A similar emission peak has been observed for H-minority heating [40] and explained to be caused by an inverted energy distribution of high-energy H-ions at the plasma edge [41].

Further indications of fast ions could be deduced from magnetic fluctuation spectrograms measured with magnetic pick up coils at the plasma edge [42]. This was best observed in the reference Pulse No: 58680 with +90° phasing without NBI and indicated that TAE modes were excited by fast ions in the frequency range of 100-200kHz.

The presence of fast ions can also be indicated by measuring the anisotropic energy content in the plasma by comparing the difference between the measured diamagnetic energy, $W_{dia} = 3W_{perp}/2$, and the equilibrium MHD energy constructed from magnetic probe measurements, $W_{MHD} = 3W_{perp}/4 + 3W_{||}/2$. The energy of the anisotropically heated fast ions corresponds to $W_{fast} = 4/3\ (W_{dia} - W_{MHD})$ [43]. Unfortunately the lack of accuracy in these measurements, and the anisotropic energy content of the beam ions, make the results uncertain. The fast energy content was found to be of the order 0.1MJ higher for +90° phasing than for –90° phasing and the central electron temperature was also found to be higher, Fig.2. Both effects are in agreement with the better central heating with +90° phasing due to the inward pinch of ion cyclotron resonant ions.

The power absorbed on ^{3}He ions but not lost to the wall could, in principal, be estimated from measurements of the fast energy content using the relation $W_{fast} = p_e\langle t_s\rangle/2$, where $\langle t_s\rangle$ is the slowing down time averaged over the distribution function and p_e is the power absorbed by ^{3}He and transferred to the electrons via collisions. Using the central slowing down time of around 0.7s in these discharges a difference of 0.1MJ between +90° and –90° phasing would indicate a difference in power absorbed by ^{3}He and not lost to the wall of around 0.3MW.

3.3 LOSS OF POWER

The fraction of time integrated RF-power that is not absorbed and transferred to the bulk plasma can in principle be obtained from the balance between the energy delivered by the heating systems, including ohmic heating and excluding beam shine-through, and the energy delivered to the divertor and radiated from the plasma. The energy delivered to the divertor can in JET be measured with 6 thermocouplers and the energy radiated from the plasma can be measured with a bolometer camera. Good balance is in general found between the total heating energy and the energy accounted for by the thermocouplers and bolometer for standard heating scenarios. For pulses dominated by ICRH the method offers a good measure of the lost power, such as in Pulse No: 58680 without NBI where 30MJ (61%) of the total delivered heating energy of 49MJ came from the RF system. Evidence of lost power could clearly be found in this discharge. 18MJ (36% of the total heating) was accounted for by the thermocouplers, 17MJ (35%) was measured by the bolometers and 14MJ (29%) was not accounted for. The lost energy corresponds to 48% of the injected RF energy and is well above the error bars for the method, ±13 percentage units for this discharge as derived from the normal levels

of accuracy of the experimental signals. Likely causes of the lost RF power are losses of RF-heated high-energy ions intercepted by the wall or the limiters and energy dissipated in rectified RF-sheaths at the antennas and the wall.

Uncertainties in the measured quantities, particularly the energy going into the divertor and the radiated energy, make the assumption that any imbalance is due to lost RF-energy less appropriate when the RF constitutes a smaller fraction of the total heating. The accuracy in the measured balance for discharges with both ICRH and NBI heating can be estimated from a heating scenario expected to work well, such as Pulse No: 58682 with hydrogen minority heating at 51MHz with +90° phasing. For this discharge 109MJ was delivered by the heating systems, excluding beam shine-through as calculated with the PENCIL code, 75MJ (69%) was delivered to the divertor and 26MJ (24%) was radiated from the plasma. A nonaccountable energy of 8MJ (7%) was below the error bars of the measurements and corresponds to 21% of the 36MJ of ICRH-energy delivered by the antennas.

Due to the uncertainties in the energy balance it is only reasonable to draw conclusions regarding trends in the same series of discharges. A general trend is that the radiation and Z_{eff} was lower and the fraction of energy going to the divertor was higher for discharges with hydrogen minority heating at 51MHz or with dipole phasing at 37MHz compared to the FWCD discharges with directed spectra at 37MHz. A similar difference was found between +90° and –90°, compare the pairs Pulse No: 58679 and Pulse No: 58681, Pulse No: 60664 and Pulse No: 60665 and also Pulse No: 60676 and Pulse No: 60675.

The difference in heating efficiency between different phasings is clearly seen when comparing a triple of discharges that had very similar electron temperatures and densities during $45 < t < 46$s despite different levels of coupled RF power, Fig. 7. The average coupled power between $45 < t < 45.5$s, just before the modulation, was 4.6MW for Pulse No: 60663 with +90° phasing, 5.8MW for Pulse No: 60664 with –90° phasing and 2.9MW for Pulse No: 60667 with dipole phasing. From this we conclude that the heating efficiency is reduced to about 50% for –90° phasing and to about 60% for +90° compared to the dipole phasing. Further indications of the dependence of the phasing on the heating efficiency are visible in Fig. 2. Pulse No: 60673 with 3.1MW of coupled RF power with dipole phasing shows similar heating efficiency as Pulse No: 58682 with 4.4MW of +90° H-minority heating but 1MW less NBI. Discharges Pulse No: 60675 and Pulse No: 60676, with respectively 5.2MW with +90° phasing and 5.3MW with –90° phasing, show significantly worse performance.

A series of discharges was also made in 4He-plasmas at low NBI power, resulting in a short-lived reversed magnetic shear phase. The discharges were characterised by normal sawtoothing in the later phase and large losses of energy. One Pulse No: 62986, was carried out with a higher plasma current of 2.8MA and thereby a smaller misalignment angle between the Faraday screens and the magnetic field lines of 5°, compared to approximately 7° for the 2MA discharges. The plasma was effectively heated using +90° phasing despite a comparatively low electron temperature during the beginning of the RF-heating due to tripping of the lower hybrid preheat, Fig. 8. Compared to the similar 2MA Pulse No: 62993 using dipole phasing, Pulse No: 62986 gave a similar fraction of radiated energy, 44% compared to 47%, and fraction of energy delivered to the divertor, 58%

compared to 63%. Both discharges had positive energy balances as measured with the above described method, indicating very good heating efficiencies, and gave similar plasma heating. Similar 2MA ^{4}He discharges, Pulse No: 62981- Pulse No: 62985, using +/–90° gave 35-42% radiated energy and 53-41% energy delivered to the divertor, thus slightly lower radiation and less energy to the divertor. The energy balances for these discharges indicate between 10 and 17MJ lost energy, corresponding to 36-57% lost RF power. The plasma heating performance was much worse for these discharges compared to the 2MA dipole and the 2.8MA +90° discharges. Since the fractions of energy radiated and delivered to the divertor and the heating performance were similar we conclude that there was a genuine reduction in lost power for the 2.8MA discharge with a smaller misalignment angle.

3.4 PLASMA EDGE AND IMPURITY

Visible light spectrometers were used to study intensity variations in the CIII, CIV and BeII lines in order to assess the level of sputtering or arcing taking place at the antenna screens and limiters. Two of the spectrometers viewed along vertical lines of sight through the plasma and the divertor, one through the inner and one through the outer half of the divertor, and one spectrometer viewed through the main plasma along a horizontal line of sight. For the discharges heated with dipole phasing or using hydrogen minority heating a steady BeII line radiation intensity of the order of 3×10^{12} photons/s/cm^2/sr was observed using the spectrometers viewing the divertor. For the FWCD experiments with +90° and –90° phasings the radiation intensity varied strongly during the pulses with large spikes and frequent tripping of the RF-generators in the early phase just after the application of RF-power and in the later phase after the NBI step down. The intensity was in general lowest during the high density and high temperature phase of the discharge when the barrier expanded to 3.45m, $r/a = 0.5$, as can be seen in Fig. 9 around $t = 47.5$s. When the intensity was high, typically of the order 10^{13} photons/s/cm^2/sr, transient spikes appeared where the intensity increased to 10^{14} photons/s/cm^2/sr. In general the BeII radiation was stronger and spikier for –90° than for +90°. The BeII radiation measured with the horizontal spectrometer showed very little variation between the different discharges and was only slightly higher when the BeII radiation in the divertor increased.

The behaviour of the CIV radiation intensity in the divertor roughly followed the BeII radiation, although the intense radiation spikes did not occur at the same time. This is consistent with arcs at the beryllium Faraday screens and carbon limiters of the antennas taking place. Since the arcs reduce the RF-sheath driven potential difference between the plasma and the wall there will either be an arc at the Faraday screen or at the limiter, but not simultaneously at both.

The strong interaction at the screens and limiters resulted in a high impurity content in the plasma. Z_{eff} measured with visible Brehmsstrahlung was around 3.5 for the discharges with dipole phasing and about 4 for discharges with +/__90° phasing. The impurity level also followed the divertor BeII radiation intensity, although with a much lower variation. The density increased slightly faster with +/-90° phasing compared to with dipole phasing when the RF-power was applied, cf. Pulse No: 60663, Pulse No: 60664 and Pulse No: 60667.

3.5 EVOLUTION OF THE CURRENT PROFILES AND EVIDENCE OF CURRENT DRIVE

EFIT equilibria reconstructions constrained by MSE or Faraday rotation data showed that the discharges had inverted q-profiles, for which the poloidal flux diffuses inwards, and that the expansion of the barriers took place when q_{min} reached 2. The central q-profiles are uncertain for these equilibria since the diagnostic neutral beam line used for MSE passes below the magnetic axis. The location of some integer q-surfaces in the reversed magnetic shear region could however be confirmed by the appearance of tearing modes, e.g. in Pulse No: 58682 at R = 3.26m at t = 5.78, consistent with a q = 3 surface in the reversed shear region in the barrier. Tearing modes in the positive magnetic shear region outside the barrier appeared as well.

The evolution of the central current density, the electron temperatures at R = 2.98m and R = 3.25m and the axial and averaged density are shown in Fig.10 for Pulse No: 60667 with dipole phasing. When the LHCD is switched off and the NBI and RF are applied the density increases and the electron temperature initially decreases. The central current density also increases due to increased current diffusion and possibly also due to small tearing mode activity in the reversed magnetic shear region. When the density barrier is established at t = 4.3s, which can be seen from the deviation between the central and average density, the central current density decreases as the bootstrap current in the barrier builds up. After t = 5s the central current starts to increase due to the inward diffusion of poloidal flux and tearing mode activity in the reversed magnetic shear region. An example of the tearing modes is seen at t =5.3s, when a rapid increase in the central current takes place. Note that the central temperature is less affected than the temperature at R = 3.27m, near the rational q = 3 surface.

Studies of the effects on the central current by FWCD and heating were attempted by comparing similar pairs of discharges with similar heating powers but different ICRH phasings, e.g. Pulse No: 58679 and Pulse No: 58681 as well as Pulse No: 60676 and Pulse No: 60675. Only small changes in the central current density could however be detected from the Faraday rotation polarimeter. The pair of Pulse No: 60664 and Pulse No: 60663 had different RF-power, but similar temperatures and densities in the early part of the main heating phase, t = 4-6s. A small but clear difference in the central current density could be seen, Fig. 11, which because of the similar electron temperatures is not expected to be caused by different current diffusion rates.

4. MODELLING OF HEATING AND CURRENT DRIVE

The magnetosonic waves are expected to be damped directly by TTMP/ELD and by cyclotron damping on ^{3}He and C impurity ions and on D majority ions. The waves can also be absorbed indirectly through mode conversion to kinetic Alfvén waves near the high field side edge. Complete modelling of the driven current requires calculations of the power absorbed by TTMP/ELD, the driven steady state current and the response of the plasma current to the current drive. Calculations of the power partition between the different plasma species require self-consistent calculations of the power deposition and the non-Maxwellian ^{3}He distribution function. Unfortunately, the lack of

accurate data for the ^{3}He concentration and for the fraction of power absorbed outside the plasma or at the plasma edge makes it difficult to accurately calculate the power partition. However, comparisons with the experiments can be done at different levels, e.g. the driven steady state current can be computed by using as input data the power absorbed directly on the electrons as measured with the modulation technique. From this the plasma current response can be calculated and compared with the measured difference in central current density between discharges with co and counter current drive. In absence of accurate data of the ^{3}He concentration and the fraction of the power absorbed in the centre of the plasma estimates of the maximum power lost by fast ions intercepted by the wall can be done by scanning the concentration.

The triple of Pulse No: 60663 with +90° phasing, Pulse No: 60664 with -90° phasing and Pulse No: 60667 with dipole phasing is used for comparison with numerical modelling. The evolution of the discharges during the first 2s after the onset of ICRH and NBI heating were quite similar and the experimental profiles for Pulse No: 60663 and Pulse No: 60664 could be regarded as identical for this period. Pulse No: 60667 had initially a little lower density and higher electron temperature. Around t = 5.5s, before the power modulation periods, all discharges had similar plasmas despite the different coupled ICRH powers of 4.6MW for the +90°, 5.8MW for -90° and 2.9MW for the dipole, Fig.7. The modulation for Pulse No: 60663 did however not start until t = 6.5s, after the NBI step down, and for comparison with the measured direct electron damping we therefore use data from the very similar Pulse No: 60665.

The driven currents are calculated with the LION code [44-46] for a reconstructed experimental equilibrium. The power is normalised so that the calculated power absorbed on electrons by TTMP/ELD agree with that measured. For these discharges 9-10% of the total power is absorbed on electrons in the centre of the plasma, which according to LION corresponds to a total electron absorption in the plasma of around 17%. The power absorbed by TTMP/ELD was for +90° 0.8MW and for –90° 1MW, yielding driven currents of –55kA and 70kA respectively. The corresponding current drive efficiencies are of the order 0.07A per watt absorbed on the electrons.

The effect of the current drive on the evolution of the central plasma current was simulated with the JETTO code [47]. In order to clearly quantify the effects of the current drive the same pulse, No: 60664, was simulated with both co and counter current drive, e.g. +70kA respectively -55kA, as well as without current drive for reference. The simulation was started at t = 4.7s, well before the power modulation at t = 5.5, and lasted until the onset of the ITB around 2.6s later. The resulting plasma current profiles due to RF, NBI and bootstrap currents and poloidal flux diffusion are shown in Fig.12. The total plasma current in the centre changes only with a small fraction of the RF driven current. After 2.6s the differences in current density inside r/a = 0.3 compared to the reference simulation without current drive are of the order +10kA/m^2 to +30kA/m^2 for co current drive and –10kA/m^2 to –15kA/m^2 for counter current. Right at the magnetic axis the difference in current density between the two current drive simulations is about 130kA/m^2. This should be compared to the driven current densities calculated with LION, which are around +80kA/m^2 and –70kA/m^2

respectively at r/a = 0.3 and increases to about +400kA/m^2 and –300kA/m^2 at the magnetic axis. Owing to the inductive nature of the plasma current the application of fast wave current drive results in an immediate change in the local electric field such that the net current density is left unchanged.

An effect of the driven current is not seen until this back EMF diffuses away, which in the high conductivity of plasmas with high electron temperatures can take quite a long time. This effect is expected to be symmetric for the two phasings for the same amount of power absorbed by TTMP/ELD. In addition, the RF driven current is also partly compensated for by an opposite change in the bootstrap current due to the dependence of the bootstrap current on the poloidal field, which is an asymmetric effect, and is the reason of the difference in response for co and counter current drive. Halfway into the simulation, at t = 6s, the total difference in the calculated central current density is only between 10kA/m^2 and 40kA/m^2 between co and counter current drive simulations. Measurements of the central current density in the corresponding –90° and +90° discharges using the Faraday rotation polarimeter however showed a difference in current density of around 100kA/m^2 at this time, as can be seen in Fig.11. This indicates that poloidal flux diffusion takes place on a faster time scale than that given by neo-classical resistivity.

The possible effects of residual ^{3}He on the performance of the discharges was investigated using the SELFO code [48, 49], which self-consistently simulates the wave field using the LION code and the distribution functions of cyclotron resonant ion species, including the effects of RF-induced spatial transport and finite drift orbit widths, using the FIDO code [50]. For the Pulse No: 60663, Pulse No: 60664 and Pulse No: 60667 the maximum possible losses of RF power with fast ^{3}He ions hitting the wall was estimated by scanning the ^{3}He impurity content from 0.01% to 0.5% of the background D density at full RF power, 2.9MW, 5.8MW and 4.6MW respectively, using the experimental profiles just before the start of the modulation at 5.5s. When artificially recycling lost ions to the plasma and running the simulations to steady-state the maximum fraction of the RF power that was lost was about 25% at 0.1% ^{3}He for the +90°phasing and about 30% at 0.2% ^{3}He for the dipole phasing. For the –90° phasing the losses increased monotonically with increasing ^{3}He concentration in the scan and were around 40% at 0.5% ^{3}He. Without any recycling a 0.5% ^{3}He concentration was completely depleted on a time scale of about 2s for all three phasings. Since it is highly unlikely that the ^{3}He impurity concentration was above 0.5% in the experiments, and since a very fast recycling of lost ions would have been necessary in order to approach the calculated maximum losses, it seems unlikely that RF power lost with fast ions was the dominant reason for the degraded heating. We therefore assume that only 2.9MW is absorbed in the plasma for the +90° and – 90° phasings, in line with the observed similar heating efficiencies of Pulse No: 60663, Pulse No: 60664 and Pulse No: 60667 and good observed heating efficiency with the dipole phasing in general. Under this assumption the maximum losses for the +/–90° phasings comes to just over 20% (of 2.9MW), Fig.13. The measured difference in fast energy content of not much more than 0.1MJ between the +90° and –90° phasings is according to SELFO for these simulations inconsistent

with a steady-state ^{3}He concentration much above 0.1%. At that concentration the calculated fast energy content with the +90° phasing was around 0.13MJ and with the –90° and dipole phasings about 0.02MJ. The RF power was in the simulations predominantly partitioned between the electrons and the ^{3}He, Fig.13. Less than a percent of the RF power was absorbed by cyclotron damping on majority D and impurity C ions. For the –90° and dipole phasings the RF power was roughly equally partitioned between electrons and ^{3}He ions for a ^{3}He concentration of 0.4%. For the +90° phasing they were equally partitioned already around a ^{3}He concentration of 0.05% due to the RF-induced inward pinch. At 0.1% ^{3}He concentration the power absorbed by electrons was about 35% with the +90° phasing, 80% with the –90° phasing and 70% with the dipole phasing.

In order to correlate power losses with the single pass damping we note that the single pass damping is not a well-defined quantity for a 2D wave field and hence not available from LION. The single pass damping for the dominant toroidal mode number is calculated for a thermal plasma with a ray tracing code, using a single ray passing along the midplane. For the pulses under comparison the single pass damping coefficients at t = 5.5s were, for thermal plasmas, 0.4% for ^{3}He damping at a concentration of 0.1% ^{3}He, and 2.3% for electron damping with +/–90° phasing. The corresponding coefficients for the dipole phasing were 0.2% for ^{3}He damping and 1.8% for electron damping. The weak single pass damping on ^{3}He is due to the low concentration and the relatively low damping on electrons is due to the low electron density and the high magnetic field. To estimate the single pass damping for the strongly non-Maxwellian distribution functions obtained through the self-consistent calculations of power deposition and wave fields we assume the single pass damping to scale with the power partition as $a_i / (a_i + a_e) = P_i / (P_i + P_e)$, where a_i and a_e is the damping and P_i and P_e is the total power absorbed by species i and electrons respectively. Taking P_i and P_e from the power partitions given by SELFO we obtain that as the distribution functions of ^{3}He reaches steady state the total single pass damping increases to about 3 - 7%, with the higher value for +90° and the lower value for –90° and the dipole.

5. DISCUSSION

A clear difference in the heating efficiency with respect to the phasing was seen. It was most clearly seen when comparing heating at different power levels producing similar plasmas. The dipole phasing had the highest heating efficiency, comparable to that of hydrogen minority heating. Pulse No: 60673, with dipole phasing at 37MHz and 3.1MW of coupled RF power, showed a higher electron temperature than did Pulse No: 58682 with 4.4MW of hydrogen minority heating and 1MW less NBI power. Fig.2. Differences in direct electron heating, lost power, production of impurities, fast ions and gamma-rays were also seen with respect to +90° and –90° phasings of the antennas for 37MHz, although these differences were smaller than those between the dipole and +/–90°. For instance, Pulse No: 60663 with +90°, Pulse No:60664 with –90° and Pulse No:60667 with dipole phasing produced very similar plasmas with respectively 4.6MW, 5.8MW and 2.9MW of coupled power. The differences between +90° and –90° are consistent with the effect of the RF-

induced spatial transport on the heating of residual ^{3}He ions. Higher electron temperatures were in general seen with +90° than with –90°. The differences in heating between dipole and +/–90° phasings could not be explained by losses of high-energy ions intercepted by the wall or the antennas, although such losses could contribute to part of the observed energy imbalance.

The power losses measured from the imbalance in the energy delivered by the heating systems and the energy radiated from the plasma into the main vessel and that delivered to the divertor cannot come from power being absorbed and transferred to the plasma inside the last closed flux surface or in the SOL region connected to the divertor through magnetic field lines. The losses have to be caused either by absorption at the RF-antennas and at the walls, e.g. in rectified RF-sheath potentials, or by fast ions heated in the plasma and intercepted by the walls and the antennas or delivered asymmetrically to the divertor in a way such that the power is not accounted for.

The experimental results demonstrate a strong correlation between lost power and single pass damping for the +/–90° antenna phasings, with large losses for scenarios with damping below 10%. This is most clearly seen by comparing heating with the same antenna phasing but different single pass damping. Only small losses were seen in Pulse No: 58682 with hydrogen minority heating where the single pass damping was around 60% whereas larger losses were seen when the single pass damping was only a few percent, as for Pulse No: 58681 and Pulse No: 58679. Differences in single pass damping are expected between +90° and –90° phasing because of the differences in the RF-induced spatial transport, with lower single pass damping for –90° consistent with a slightly larger energy loss. The single pass damping with the dipole phasing, which provided efficient heating, was even lower than with the +/–90° phasings.

Mode conversion near the high field side edge is a possible mechanism for degrading the heating. It could occur in these FWCD experiments and explain part of the heating degradation, although it cannot explain the large fraction of unaccountable energy. That the main degradation of the heating is caused by absorption via mode conversion is also inconsistent with the significant improvement in heating performance and reduction in energy imbalance observed in Pulse No: 62986, when the plasma current was increased from 2 to 2.8MA, since the mode conversion is expected to be unaffected by the plasma current. A recent investigation of the reduced heating efficiency with monopole phasing for hydrogen minority heating also observed similar energy imbalances with the monopole phasing, whereas heating with the dipole phasing was not degraded [14]. Since the wave frequency in those experiments was above the fundamental cyclotron frequency of deuterium in the whole plasma these losses could not have been caused by mode conversion. Neither can the losses be explained by losses of fast hydrogen ions since the RF power was low and the hydrogen to deuterium concentration was of the order of 2%, which is sufficiently high for the losses of fast hydrogen ions to be negligible.

The possibility that heating of beam ions is the main cause of the degradation is not consistent with the absence of gamma-rays arising from high-energy deuterium ions heated at the fundamental deuterium cyclotron resonance. Such gamma-rays have been seen in the past in mode conversion experiments [31].

Simulations indicate that a fraction of the power is lost to the walls with fast ^{3}He ions, but that this fraction is too small to fully explain the measured energy imbalances. It is conceivable however that the improved heating observed in Pulse No: 62986 with 2.8MA plasma current in a series of discharges with 1.5MW hydrogen minority heating in addition to the current drive may in part have been due to decreased losses of fast hydrogen ions.

The large differences between the dipole and +/–90° phasings with respect to the BeII and CIV line radiation in the divertor are consistent with intense interactions near the antennas and the limiters by RF-rectified sheath potentials with the +/–90° phasings, and with very little interaction with the dipole. The +/–90° phasings, and in particular the –90° phasing, produce strong radiation with frequent spikes in the intensity. A clear correlation between the expected variation of the single pass damping and the intensity was seen with +90° and –90° phasings. Frequent spikes appeared when the single pass damping was weak and when the coupling of the RF-system was less well matched. After the beam step down the radiation increased, in particular for the –90° phasing, with frequent spikes in the BeII line intensity, Fig.9. The lowest intensity was when the barrier expanded and the single pass damping for TTMP/ELD is expected to have been the highest, as was the case at t = 7.5s for Pulse No: 60664 in Fig.9. The BeII line radiation was also much lower for H minority heating at 51MHz with the +90° phasing and strong single pass damping. Similar spikes in the radiation intensity have been observed with two of the antennas in dipole phasing and two in monopole phasing with different phases of the adjacent antennas [51], and for large misalignment angles between the Faraday screens and magnetic field [17]. The spikes in the radiation intensity were in these cases concluded to be likely to have been caused by arcing. Arcs should appear when the rectified sheath voltage and the temperature of the surface are sufficiently high so that electrons can be accelerated out of the surface [51].

Direct losses at the antennas and walls in the presence of rectified RF-sheath potentials can provide a common explanation for the degradation of the different heating scenarios. Rectified RF-sheath potentials are formed when electrons are accelerated along magnetic field lines by parallel electric fields into conducting surfaces. The rectified RF-sheath potentials are then dissipated by ions accelerated along the field lines into the conducting surfaces. The amount of power which is lost is determined by the rectified sheath potential and the ion saturation current. The latter is proportional to the square root of the electron temperature and to the plasma density, both of which are affected by sputtering and transport by convective cells caused by the inhomogeneity of the rectified RF-sheath potential, making the process non-linear. The potential function driving the rectified sheath increases with misalignment angle, antenna voltage and enclosed flux. In a multi-strap antenna the flux, and hence the driving potential, depends on the phase difference between the currents in different straps. The largest driving voltage is obtained in the absence of a phase difference, i.e. for monopole phasing. The lowest voltage is obtained for dipole phasing, when adjacent straps are phased oppositely. The driving voltages for +/–90° phasings are between those of the monopole and dipole phasings. A gradual increase in the heating efficiency was seen

for the JET A2 antennas with an increasing magnitude of the phase difference from 0° to 180° [13], qualitatively consistent with a reduced sheath driving voltage.

Earlier experiments in JET using the A1 antennas with large misalignment angles of 22° showed small losses with the dipole phasing [16] but strong degradation of the heating with the monopole [16, 17], consistent with losses at rectified RF-sheath potentials at the Faraday screens [17]. The power losses in these experiments were found to be proportional to the coupled power. Strong impurity releases from the nickel antennas [16, 18] and beryllium screens [17] were seen, and even further increased in conjunction with arcs [17]. Invessel inspection of the antennas later revealed that the entire screens had been subjected to sputtering. The main contribution to the screen sputtering and corresponding power dissipation had come from the front face of the screen [17]. Results with small misalignment angles indicated that the heating efficiency of the JET A1 antennas was approximately independent of antenna phasing [15]. The heating efficiencies in experiments with low single pass damping in monopole phasing were however shown to be degraded with respect to single pass damping [52, 53].

A misalignment angle of 25° was not found to cause severe losses in FWCD experiments in DIII-D [7]. However, the single pass damping in the FWCD experiments in DIII-D in L-mode was in general larger than in the present FWCD experiments in JET. Nevertheless modelling of the DIII-D FWCD experiments required an ad hoc damping corresponding to a single pass damping of 4% in order to get agreement with the experiments. For plasmas heated with ECE a higher damping was required, qualitatively consistent with higher ion saturation currents. In H-mode the scaling with single pass damping was not critical in FWCD experiments in DIII-D [8], instead the ELM frequency was the most important parameter. The losses could be reduced by increasing the distance between the antenna and the plasma. These results are at least in qualitative agreement with losses caused by the dissipation of rectified RF-sheath potentials because of the strong dependence of the losses on the plasma density near the antennas and the walls.

The concentration of the impurity ^{3}He is a critical parameter for determining the single pass damping, the power partition and the ^{3}He distribution function. ^{3}He concentrations in the experiments were low and difficult to estimate, the active charge exchange spectroscopy measurements indicated a concentration below 0.5%. The measured fast energy contents were also low and had consequently large error bars, consistent with a rather low concentration of ^{3}He. It is likely that the concentration varied between the different experimental campaigns when the experiments were performed. The modelled and measured direct electron power depositions and the differences in fast energy content between the discharges agree fairly well for an assumed concentration of around 0.1% ^{3}He in the series of Pulse No: 60661 - Pulse No: 60676.

The single pass damping for thermal plasmas heated with 37MHz with concentrations around 0.1% of ^{3}He is dominated by direct electron damping by TTMP/ELD. When the high-energy tail develops on the distribution function of the ^{3}He ions the damping on ^{3}He increases and becomes comparable to TTMP/ELD. Because of the RF-induced spatial transport of resonant ions the single

pass damping becomes stronger for +90° phasing, for which ^{3}He ions are accumulated in the centre, compared to –90°, for which they are thrown out from the centre. In connection with the beam step down the single pass damping on electrons decreases as the barrier contracts and the density and the electron temperature decrease.

The fraction of the power absorbed by direct electron heating obtained from modulations is seen to increase with the single pass damping for TTMP/ELD and to decrease with the single pass damping for ^{3}He. This can be seen by comparing the early part of the main heating phase of the pair Pulse No: 60665 with +90° and Pulse No: 60664 with –90° and the pair Pulse No: 60675 with +90° and Pulse No: 60676 with –90°. The fraction of direct electron heating is often smaller for +90° than for –90°, despite an often higher electron temperature for +90° as was the case for Pulse No: 60675 and Pulse No: 60676. The uncertainties in the ^{3}He concentration and of the fraction of power absorbed in the plasma were large, and the fact that the losses could be due both to rectified RF-sheath potentials and losses of heated fast ions made the simulations difficult. The uncertainty of the power absorbed in the plasma was largely due to the error bars in the measured fraction of the time integrated power absorbed in the plasma and the variation of the absorption during the discharge.

The modelling with the JETTO code demonstrates the difficulty in affecting the current in the transport barrier because of the interplay between the driven current and the bootstrap current and because of the inductive nature of plasmas with high electron temperatures and the resulting long diffusion times for the poloidal flux. The simulations predict only small changes in the currents near the magnetic axis after 2.6s of diffusion. The changes in the current profile by the changes in bootstrap currents as well as the differences in TTMP/ELD damping caused by resonant ^{3}He ions result in asymmetric current drive efficiencies with respect to the phasing. Asymmetries in current drive efficiencies between co and counter current drive have previously been observed in experiments on DIII-D [10] and Tore Supra [9]. The difference in central current density during co and counter current drive as measured from Faraday rotation is, although still smaller than the difference between the steady state driven currents, much larger than the difference in the response of the plasma current as calculated with the JETTO code. This suggests a much shorter current penetration time than that given by neo-classical resistivity. The differences cannot solely be explained by a larger fraction of power being absorbed by TTMP/ ELD since that would require that nearly all the power is absorbed by TTMP/ELD and contradict both the measured direct electron damping and the reduced heating efficiency of about 50% with the +/–90° phasings compared to the dipole phasing. Fast changes in the current profile by the redistribution of current by MHD events are seen, and could be a reason for the larger difference in measured central current density.

6. CONCLUSIONS

Direct electron heating by fast magnetosonic waves using dipole spectra has proven to be an effective method to heat electrons in these ITB plasmas with strongly reversed magnetic shear in JET, comparable to H-minority heating. Direct electron heating has the advantage over indirect heating

via cyclotron heated high-energy ions of a prompt heating without increasing the fast ion pressure. Due to low current density inside the strongly reversed magnetic shear region it provides a more peaked heating profile than minority heating can achieve because of the broad orbits of the heated ions. However, the heating and current drive in FWCD experiments in ITB plasmas as described in preceding sections is strongly degraded by parasitic losses and have an efficiency of about half that of the dipole. Direct evidence of this is obtained by observing that a large fraction of the power coupled by the antennas is not absorbed and transferred to the bulk plasma. This is found by comparing the energy delivered by the heating systems, including time integrated ohmic power and excluding NBI shinethrough losses, with the sum of the radiated energy and the energy delivered to the divertor. The fraction of power absorbed in the plasma increases with single pass damping and depends on the phasing. Parasitic losses due to absorption on resonant residual ^{3}He ions were seen. Losses by fast ^{3}He ions were detected with a probe outside the plasma and such losses are also predicted from simulations with the SELFO code. The calculated losses with fast ions were however much smaller than the energy losses experimentally observed. The fraction of unaccountable energy was in general larger for –90° than for +90°, whereas the RF power absorbed directly on electrons as obtained from power modulations was, in general, equal or larger for –90° in similar plasmas. This is at least qualitatively consistent with a stronger single pass damping for the inward RF-pinch of the ^{3}He tail with +90° compared to that obtained with the inverted RF-pinch directed outwards for –90°.

Observations supporting that the losses are primarily caused by the presence of rectified RF-sheath potentials come from the differences in BeII line radiation intensities and the large differences in performance between the dipole and +/–90° phasings. In addition, the calculated maximum losses of fast ions are for all phasings smaller than the observed imbalance in energy. The correlation of the losses with the misalignment angle between the Faraday screens and the magnetic field for weak single pass damping provides further support that the imbalance is primarily caused by the presence of rectified RF-sheath potentials and not by losses of fast ^{3}He ions. The strongest Be interactions take place in the early phase before the tail has developed and the single pass damping is low, and also after the beam step down when the electron temperature and hence the single pass damping is low. The BeII line radiation for +/–90° phasing goes down to a level similar to that during dipole heating when the barrier expands and a hotter and denser plasma is formed in the centre.

Because of the inductive nature of plasmas with high electron temperatures it is difficult to affect the current in the transport barrier, and in particular driving counter current because of the interplay between the RF-driven current and the bootstrap current. The measured difference in central current density for co and counter current drive is larger than the modelled response on the plasma current to the current drive, but smaller than the calculated steady state current drive. This suggests a faster current penetration time than that given by the neo-classical resistivity.

Fast wave current drive in this frequency range seems more promising for ITER and future reactors since the expected single pass damping will be higher, due to the size of the plasma, the

higher electron density and the higher temperature. Hence the parasitic losses caused by rectified RF-sheath potentials and by fast ions intercepted by the wall will be smaller. Good alignment between the magnetic field and the Faraday screen may still be important though. Avoiding cyclotron interactions would still be difficult in ITER for this scenario however since the second harmonic tritium resonance is located at the same position as that for fundamental ^{3}He.

REFERENCES

[1]. D.J.M. Wort, 1971 *Plasma Physics* **13** 258

[2]. T. Stix, 1975 *Nuclear Fusion* **15** 737

[3]. R.J. Bickerton, *et al* 1971 *Nature Phys. Sci.* **229** 110

[4]. S.C. Chiu, V.S. Chan, R.M. Harvey, and M. Porkolab, 1989 *Nuclear Fusion* **29** 2175

[5]. N. Hawkes, *et al* 2001 *Phys. Rev. Lett*. **87** 115001

[6]. L.-G. Eriksson, and T. Hellsten, 1989 *Nuclear Fusion* **29** 875

[7]. C.C. Petty, *et al* 1995 *Nuclear Fusion* **35** 773

[8]. C.C. Petty, *et al* 1999 *Nuclear Fusion* **39** 1421

[9]. E.T. Supra, and B. Soutic, 1994 *Plasma Physics and Controlled Fusion* **36** B123

[10]. R.Prater, M.E. Austin, F.W. Baity, S.C. Chiu, R.W. Callis, *et al* 1996 in *Proc. 16th IAEA Int. Conf. On Plasma Physics and Controlled Fusion Research*, Montreal, Vol. 3, pp 243

[11]. L.-G. Eriksson, *et al* 1998 *Nuclear Fusion* **38** 265

[12]. M.J. Mantsinen, *et al* 2002 *Phys. Rev. Lett.* **89** 115004

[13]. J. Hedin, "Studies of heating efficiencies and models of RF-sheaths for the JET antennae", *Technical report Royal Institute of Technology* TRITA-ALF-1996-01, ISN 1102-2051

[14]. J. Heikkinen, V.V.Bobkov, D.A. D'Ippolito, *et al* Experiments on ICRF coupling with different phasings, 2004 *31st EPS on Controlled Fusion Plasma Physics*.

[15]. J.J. Jacquinot, and the JET team 1988 *Plasma Physics Controlled Fusion* **30** 1467

[16]. M. Bures, Jacquinot, J.J., Start, D.F.H., and Brambilla, M., 1990 *Nuclear Fusion* **30** 251

[17]. M. Bures, J.J. Jacquinot, M.F. Stamp, D.D.R. Summers, D.F.H. Start, Wade, T. D'Ippolito, D.A., Myra, J. R., 199*2 Nuclear Fusion* **32** 1139

[18]. M. Bures, J.J. Jacquinot, K. Lawson, M.F. Stamp, D.D.R. Summers, D.A. D'Ippolito, J.R. Myra, 1991 *Plasma Physics and Controlled Fusion* **33** 937

[19]. F.W. Perkins, 1989 *Nuclear Fusion* **29** 583

[20]. M. Brambilla, R. Chodura, J. Hoffmann, et al., 1991 "Theoretical and experimental investigation of a mechanism for impurity production by ICRF fields'', *Plasma physics and Controlled Nuclear Fusion Research,* (13th. IAEA Conference, Washington, 1990), Vol. 1, IAEA(Vienna) 723.

[21]. T. Hellsten, and M. Laxåback, 2003 *15th RF Topical Conf. on Radio Frequency Powers in Plasmas*, Wyoming, Moran, pp 110

[22]. T. Hellsten, and M. Laxåback, submitted to Physics of Plasmas.

[23]. M.J. Alava, J.A. Heikkinen, and T. Hellsten, 1995 *Nuclear Fusion* **35** 881

[24]. D. Van Eester, *et al* 2002 *Nuclear. Fusion* **42** 310

[25]. T. Hellsten, *et al* 2001 *28th EPS on Controlled Fusion Plasma Physics* pp. 174.
[26]. L. Chen, J. Vaclavik, and G.W. Hammett, 1988 *Nuclear Fusion* **28**, 389
[27]. M. A. Kovanen, W.G. F. Core, and T. Hellsten, 1992 *Nuclear Fusion* **32**, 787
[28]. L.-G. Eriksson, *et al* 1998 *Phys. Rev. Lett*. **81** 1231
[29]. A. Key, *et al* 1994 *Fusion Enginering and Design* **24** 1
[30]. D.J. Gambier, *et al* 1990 *Nuclear Fusion* **20** 23
[31]. M.J. Mantsinen, *et al* 2004 *Nuclear Fusion* **44** 33
[32]. R. Bartiromo, *et al* 1989 *Rev. Sci. Instruments* **60** 237
[33]. N.C. Hawkes, *et al* 1999 *Rev. Sci. Instruments*. **70** 894
[34]. L. Lao, *et al* 1990 *Nuclear Fusion* **30** 1035
[35]. D. Mazon, *et al* 2002 *Plasma Physics and Controlled Fusion* **44** 1087
[36]. G. Bonheure, *et al* 2003 "Report on the Escaping MeV ion losses measurements based on Activation technique during C9 JET campaign", *JET internal report* EFDA-JET-R(03)01
[37]. D.J. Campbell, D.F.H. Start, J.A. Wesson, *et al* 1987 *Phys. Rev. Lett.* **60** 2148
[38]. E. Joffrin, *et al* 2003 *Nuclear Fusion* **43** 1167
[39]. V.G. Kiptily, *et al* 2002 *Nuclear Fusion* **42**, 999
[40]. G.A. Cottrell, 2000 *Phys. Rev. Lett*. **84** 2397
[41]. B. Coppi, 1993 *Phys. Lett*. **A172** 439
[42]. A. Fasoli, *et al* 1997 *Plasma Physics and Controlled Fusion* **39** (suppl 12B) B287
[43]. J.P. Christiansen, 1987 *J. Computer Phys*. **73** 85
[44]. L. Villard, *et al* 1986 *Computer Physics Reports*, **4** 95
[45]. L. Villard, *et al* 1995 *Nuclear Fusion* **35** 1173
[46]. T. Hellsten and L.-G. Eriksson, 1991 in Proc. IAEA Technical Committee Meeting on Fast Wave Current Drive in Reactor Scale Tokamaks, Arles, France.
[47]. T. Tala, *et al* 2000 *Nuclear Fusion* **40** 1635
[48]. J. Hedin, T. Hellsten, and J. Carlsson, 1998 in *Proc. of Joint Varennna-Lausanne Workshop* "*Theory of Fusion Plasmas*" pp. 467, Varenna ISBN 88-7794-167-7
[49]. J. Hedin, *et al* 1998 *Plasma Physics and Controlled Fusion* **40** 1085
[50]. J. Carlsson, *et al* 1994 in *Proc. of Joint Varennna-Lausanne Workshop* "*Theory of Fusion Plasmas*" pp.351, Varenna
[51]. D.A. D'Ippolito, J.R. Myra, P.M. Ryan, E. Righi, J. Heikkinen, P.U. Lamalle, J.-M. Noterdaeme, 2002 *Nuclear Fusion* **42** 1357
[52]. M. Bures, and K. Avinash, 1988 *Bull. Am. Phys. Soc*. **33** 2032
[53]. J.R. Myra, D.A. D'Ippolito, and M. Bures, 1994 *Physics of Plasmas* **1** 2890

No	Phase	(%) RF power accounted for	(MJ) Total heating energy	(%) RF heating energy	(%) Energy to bolo-meter	(%) Energy to Thermo-couplers	(%) Energy lost	Z_{eff}	(MW) Average RF power	(%) Direct electron damping r/a<0.5 Early/late	(KeV) T_e Early/late
58679	−90°	61+/-34	117	29	29	60	11	4.0	4.1		8.3/5.9
58680[1]	+90°	52+/-13	49	61	35	36	29	3.7	3.7		3.8/3.9
58681	+90°	69+/-34	118	29	28	63	9	3.9	4.1		8.3/6.2
58682	+90°	79+/-31	109	33	24	69	7	3.7	4.4[2]		8.1/8.1
58684	+90°	67+/-34	150	29	27	63	10	4.5	5.3		8.2/7.6
60661	−90°	54+/-42	108	23	33	56	11	3.6	4.0	11/11	6.2/6.4
60662	−90°	54+/-35	114	27	31	56	12	3.8	5.1	11/10	6.9/6.6
60663	+90°	89+/-36	91	27	39	58	3	4.1	4.0	12[3]/10	6.8/5.7
60664	−90°	65+/-30	107	31	31	59	11	4.0	5.3	10[4]/5[4]	8.2/5.4
60665	+90°	83+/-35	100	29	35	60	5	3.8	4.8	9/7	7.5/6.3
60667	180°	46+/-71	89	15	29	63	8	3.4	2.2	20[5]/	8.5/5.9
60673	180°	64+/-44	83	23	29	63	8	3.5	3.1	23/13	8.7/5.7
60674	−90°	53+/-9	102	21	30	60	10	3.6	3.4		7.2/9.9[6]/6.3[7]
60675	+90°	62+/-37	119	26	29	61	10	3.7	5.2	13/	7.6/8.3
69676	−90°	55+/-31	108	30	29	57	13	4.1	5.3	28/5	7.0/5.8
62981[8]	−90°	57+/-34	95	26	36	53	11	4.7	4.1[9]	/20	4.5/3.9
62982[8]	−90°	64+/-28	103	32	35	53	11	5.0	5.4[9]	8/	4.9/4.5
62983[8]	−90°	52+/-26	106	32	42	43	16	5.8	5.6[9]	6/7	4.2/4.0
62984[8]	+90°	50+/-27	109	32	43	41	16	5.7	5.6[9]	4[4]/12[10]	4.3/4.0
62985[8]	+90°	43+/-26	110	31	42	40	18	5.6	5.6[9]	6/	4.5/4.0
62986[8,11]	+90°	108+/-34	99	31	44	58	−3	4.9	5.4[9]	5/8	4.8/5.0
62990[8]	180°	75+/-86	72	12	40	57	3	4.0	1.5[9]		3.8/3.2
62993[8]	180°	128+/-31	89	37	47	63	−10	5.0	5.4[9]		5.7/5.0

JG05.11-14c

Table 1:

[1] *No NBI.*
[2] *Power at a frequency of 51MHz, heating of H-minority.*
[3] *Early phase around t =6s and late phase at t=9s, first modulation phase occurred after beam step down.*
[4] *Within r/a < 0.3.*
[5] *Within r/a < 0.4.*
[6] *At the peak of the expanded barrier.*
[7] *Late phase at t=10s.*
[8] *In ^{4}He plasmas.*
[9] *Including 1.5MW of power at 51MHz with dipole phasing (180°).*
[10] *Within r/a < 0.9.*
[11] *With 2.8MA plasma current.*

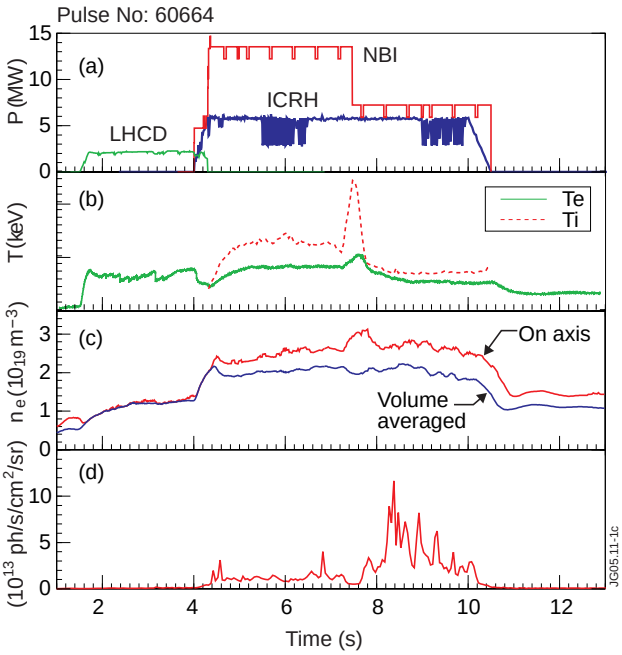

Figure 1: Time traces for Pulse No: 60664. (a) NBI, ICRF and LHCD power, (b) central electron, T_e, and ion, T_i, temperature, (c) on axis and volume averaged electron density, n_e, and (d) BeII line radiation intensity along a sight line passing through

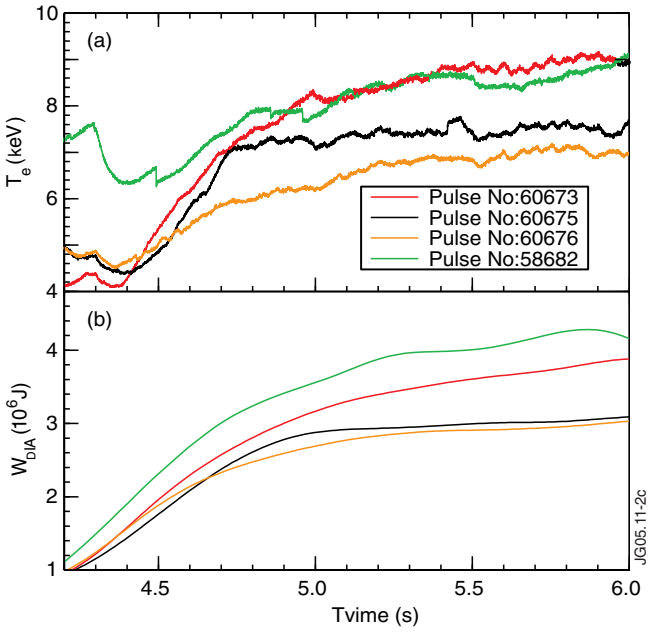

Figure 2: (a) Central electron temperatures, T_e, and (b) diamagnetic energy, W_{DIA}, for Pulse No: 58682 with 4.4MW +90° 5% hydrogen minority heating at 51MHz, Pulse No: 60673 with 3.1MW dipole, Pulse No: 60675 with 5.2MW +90° and Pulse No: 60676 with 5.3MW –90° phasing. ICRH and NBI heating start at 4.0s. The power is modulated between 5.5 and 6.5s for 60673, Pulse No: 60675 and Pulse No: 60676. The power modulation for Pulse No: 58682 takes place outside the plotted time window. Strong sawtooth-like crashes are visible for Pulse No: 58682 at 4.5, 4.85 and 4.95s.

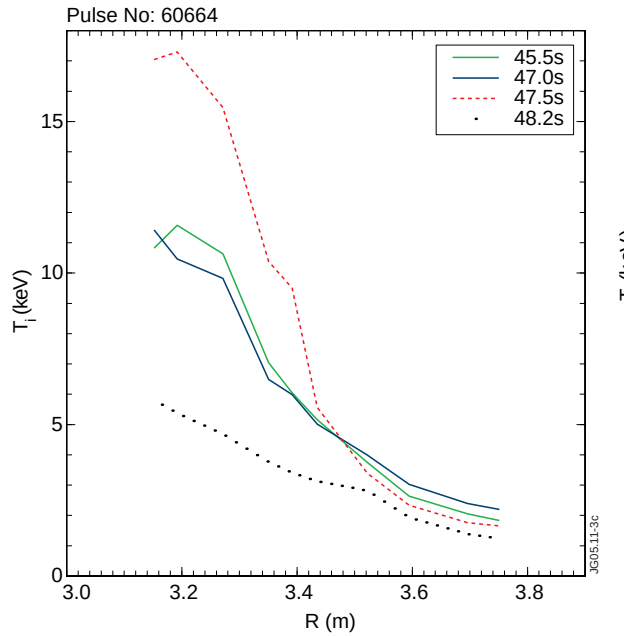

Figure 3: Ion temperature profiles for Pulse No: 60664 at 5.5, 7.0, 7.5 and 8.2s.

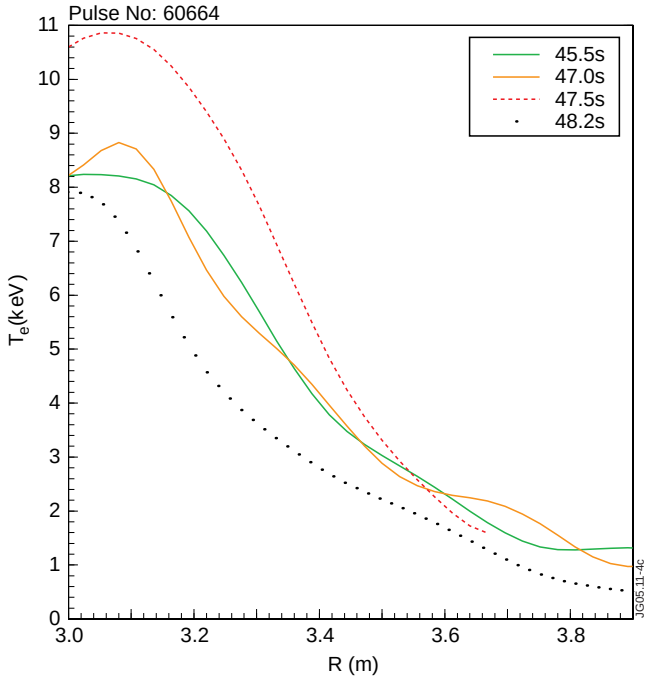

Figure 4: Electron temperature profiles for Pulse No: 60664 at 5.5, 7.0, 7.5 and 8.2s.

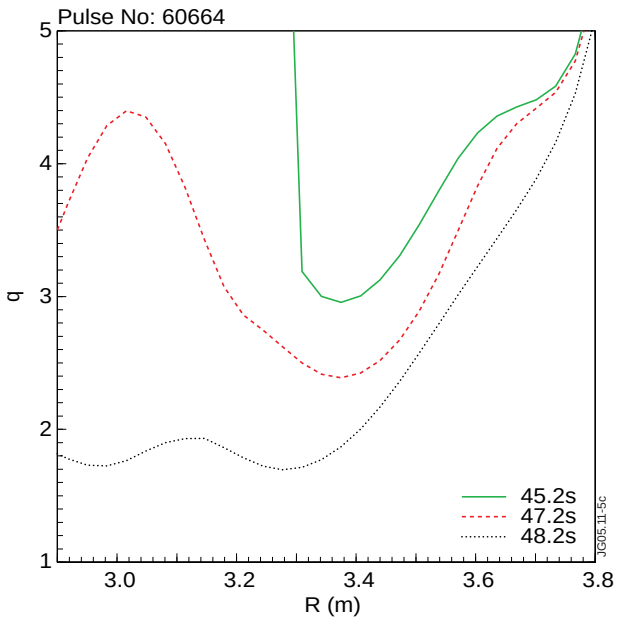

Figure 5: q*-profiles for Pulse No: 60664 measured with MSE at 5.2, 7.2 and 8.2s.*

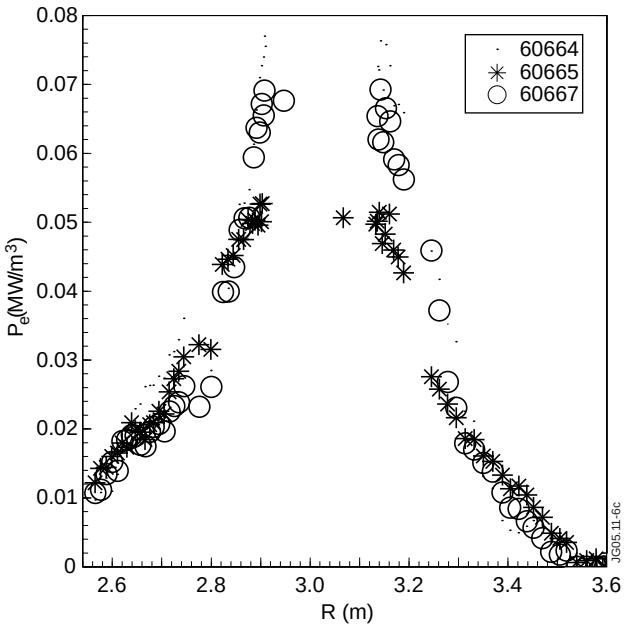

Figure 6: Power deposition through direct electron heating obtained with modulation between 5.5 and 6.5s for Pulse No: 60664 with 5.3MW –90°, Pulse No: 60665 with 4.8MW +90° and Pulse No: 60667 with 2.9MW dipole phasing.

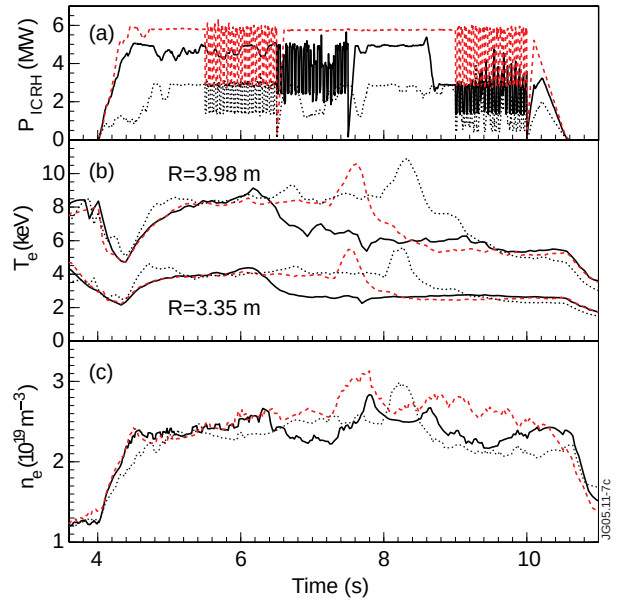

Figure 7: Comparison of (a) ICRH power, (b) electron temperatures at R *=3.0m and* R *= 3.35m and (c) central electron density for Pulse No: 60663 (full line), Pulse No: 60664 (dashed line) and Pulse No: 60667 (dotted).*

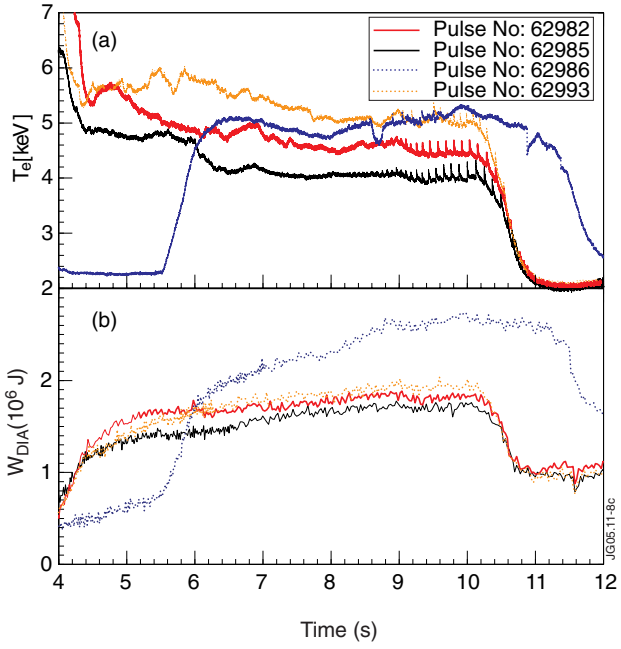

Figure 8: (a) Electron temperatures and (b) diamagnetic energy content for Pulse No: 62982 with 5.4MW -90°, Pulse No: 62985 with 5.6MW +90°, Pulse No: 62986 with 2.8MA 4.9MW +90° and Pulse No: 62993 with 5.4MW dipole. ICRH and NBI heating takes place between 4.0 and 10.5s except for Pulse No: 62986 for which it takes place between 5.5 and 11.5s. The LHCD stops at 2.1s for Pulse No: 62986 and at 4.3s for the other discharges.

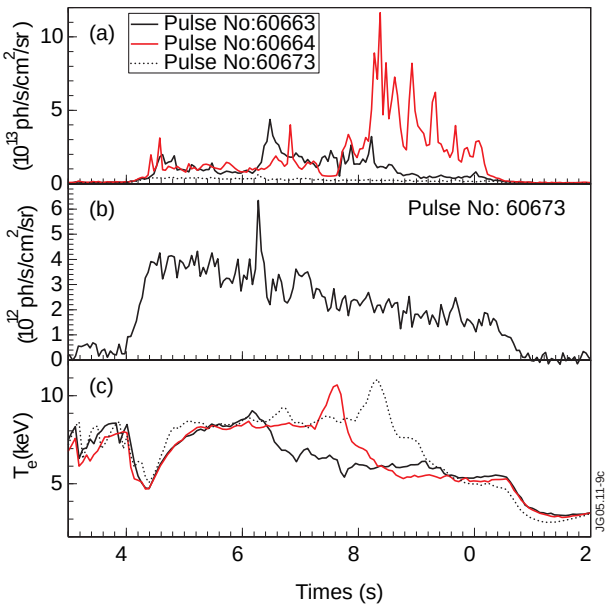

Figure 9: (a), (b) BeII line radiation intensity at the inner divertor and (c) central electron temperature for Pulse No: 60663, Pulse No: 60664 and Pulse No: 60673.

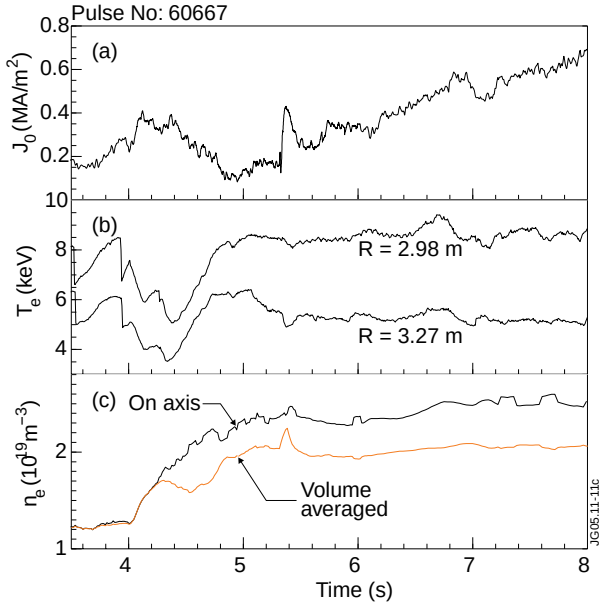

Figure 10: (a) Central current density derived from Faraday rotation, (b) electron temperature at R *= 2.98m and* R *= 3.27m and (c) axial and averaged electron densities for Pulse No: 60667 with dipole phasing.*

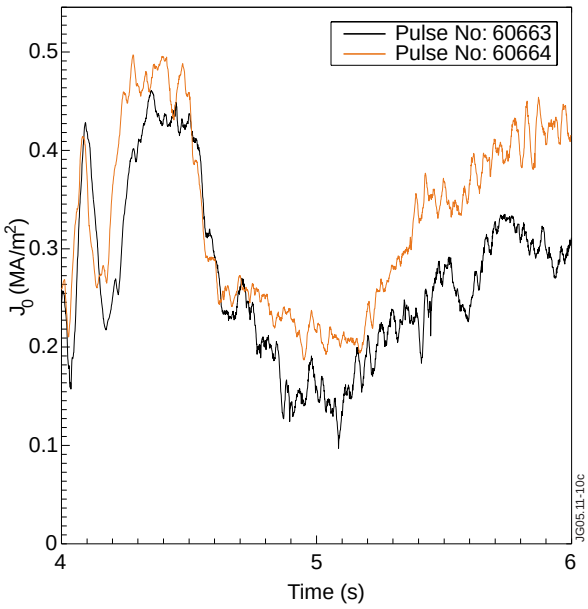

Figure 11: Central current density derived from Faraday rotation for Pulse No: 60663 with +90° and Pulse No: 60664 with –90° phasing.

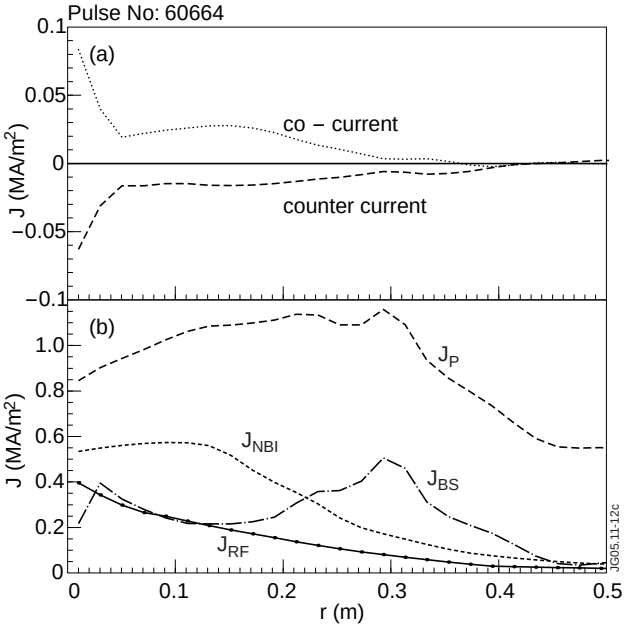

Figure 12: (a) Calculated plasma current density response to 2.6s of co- and counter-current current drive, i.e. the difference between the plasma current with and without current drive. (b) Total plasma current density, RF- and NBI-driven current densities and bootstrap current density after 2.6s of co-current current drive.

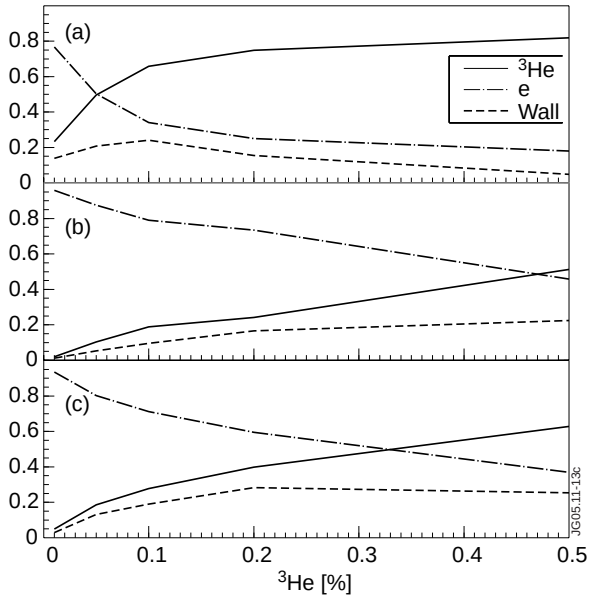

Figure 13: Calculated steady state power partition and wall losses versus ^{3}He concentration assuming 2.9MW absorbed in the plasma for (a) +90° (b) –90° and (c) dipole phasing.